

Article

The Integrated Component-System Optimization of a Typical Thermal Management System by Combining Empirical and Heat Current Methods

Junhong Hao * , Youjun Zhang  and Nian Xiong

Key Laboratory of Power Station Energy Transfer Conversion and System of Ministry of Education, School of Energy Power and Mechanical Engineering, North China Electric Power University, Beijing 102206, China; ttzzzhangyoujun@163.com (Y.Z.); 18810522732@163.com (N.X.)

* Correspondence: hjh@ncepu.edu.cn

Received: 27 October 2020; Accepted: 27 November 2020; Published: 1 December 2020



Abstract: Integration of modeling and optimization of a thermal management system simultaneously depends on heat transfer performance of the components and the topological characteristics of the system. This paper introduces a heat current method to construct the overall heat current layout of a typical double-loop thermal management system. We deduce the system heat transfer matrix as the whole system constraint based on the overall heat current layout. Moreover, we consider the influences of structural and operational parameters on the thermal hydraulic performances of each heat exchanger by combining the empirical correlations of the heat transfer and pressure drop. Finally, the minimum pressure drop is obtained by solving these optimal governing equations derived by the Lagrange multiplier method considering the physical constraints and operational conditions. The optimization results show that the minimum pressure drop reduces about 8.1% with the optimal allocation of mass flow rates of each fluid. Moreover, the impact analyses of structural and operating parameters and boundary conditions on the minimum and optimal allocation present that the combined empirical correlation-heat current method is feasible and significant for achieving integrated component-system modeling and optimization.

Keywords: thermal management system; component-system; heat current method; empirical correlation; integration optimization

1. Introduction

The thermal management system has played an increasingly essential and promising role in such fields as data center [1], building [2], electric/fuel cell vehicles [3–5], energy storage [6], and spacecraft [7,8]. For example, with the development of the Cloud service and the 5th generation wireless systems, data processing centers with high-power electric devices require a higher efficiency thermal management system. Meanwhile, with extensive utilization of electric and fuel cell systems in the transportation field, the mobile communication equipment industry, and the distributed integrated energy system, guaranteeing the optimal operation requirements of batteries (55–65 °C for electric vehicles and fuel cell vehicles [9–11]) using a thermal management system has attracted more attention. In general, a typical thermal management system consists of various heat transfer components (heat exchangers), flow equipment (pump and fan), and power and control systems (power sources). In this system, each component has its own unique physical characteristics, however, each component also generates some highly linked behaviors with other components [12], which pose significant impacts on the overall performance of the thermal management system [13]. Therefore, synergy of the component structure design and system performance optimization is essential for a comprehensive analyses of a thermal management system.

In recent years, many researchers have made significant efforts to promote the design of heat exchangers and thermal management system optimization. The former stage attached more attention to enhancing the heat transfer process [14,15], heat transfer empirical correlations for various applications [16,17], and structural parameters optimization [18–20]. The later stage focused far more on thermal system modeling and optimization by introducing entropy generation [21,22], exergy analysis [23,24], entransy dissipation [25,26], and thermoeconomics theory [27,28] combining with some heuristic algorithms [29–32]. Meanwhile, some researchers have considered heat transfer component structure in thermal system optimization and developed some solutions by combining with Computational Fluid Dynamics (CFD) simulation [33,34]. Although a CFD simulation can obtain more information about temperature, velocity, and pressure distributions of the convective heat transfer in the heat transfer component, a simulation is not straightforward. Calculating time and simulation complexity increase accompanied by an increase in heat transfer component quantity. In addition, distributions of temperature and velocity are not always necessary for system simulation and optimization in some cases. For example, local temperature, velocity, and pressure are not requisites for optimizing a building heat transport and gas refrigeration system [35]. Therefore, a suitable and feasible solution for integrating modeling and synergy optimization of components and systems in a thermal management system is highly desired.

For a heat exchanger, which is a fundamental component of a thermal management system, the corresponding empirical correlations of heat transfer factor (j -factor) and flow resistance friction factor (f -factor) by experiments or simulations are very significant and essential to its design and performance analysis. According to these corresponding empirical correlations, the log mean temperature difference (LMTD) method or the effectiveness-number of transfer units (NTU) method [36–38] are practical solutions for the design or rating problems of a single heat exchanger by introducing an implicit relationship between design parameters and requirements. However, a simple combination of empirical correlations and LMTD or effectiveness-NTU method is not suitable for thermal system integration and optimization under the conditions limited by these implicit relationships and some intermediate parameters. Recently, as an alternative to the above analysis perspective, a new heat current (power flow) method that considered the dual characteristics of the heat transfer conservation and irreversibility [39–42] was proposed. It has been widely applied to both the structural design of a single heat exchanger and the analysis and optimization of heat transfer systems for good reasons [43–46]. It directly describes the heat flux passing through the thermal resistance driven by the linear temperature difference and represents all factors that influence heat transfer performance, by an explicit relationship including the heat exchanger area, heat transfer coefficient, mass flow rates of hot and cold fluids, and the flow arrangement [42]. Therefore, a combination of empirical correlation and heat current method provides an alternative and feasible solution for the overall integration and optimization of a thermal energy system by considering the heat transfer component performance and system characteristics.

This research introduces a typical double-loop thermal management system consisting of a cross-flow plate-fin heat exchanger and a counter-flow heat exchanger, as well as a cooling plate. Then, we apply the heat current method to construct the overall heat current layout and deduce the whole heat transfer matrix by Kirchhoff's law. In the matrix, the network thermal resistance reflects the transfer and transport resistance of thermal energy. Moreover, we introduce the empirical correlations of heat transfer and flow resistance in different heat exchangers for analyzing the structural parameters of each heat exchanger as optimization variables. Finally, the minimum pressure drop is considered to be the optimization objective by considering the overall system-level heat transfer constraint and heat exchanger structure constraints. The optimization results present the feasibility of the proposed component-system optimization solution.

2. The Structure of a Typical Double-Loop Thermal Management System

Figure 1 shows a typical double-loop thermal management system used in such fields as spacecraft environment control, battery energy management, and building energy management, etc. In general, a typical double-loop thermal management system includes an internal loop heat transfer subsystem, an external loop heat transfer subsystem, and a power subsystem. To satisfy different thermal demands, such as the indoor temperature, cooling temperature, and electronic device working temperature in a thermal management system, there are various flow arrangement heat exchanges in the internal loop, as presented in Figure 1. In a thermal management system, inner-circulating fluid with a lower temperature successively flows through the cross-flow plate-fin heat exchanger (HX₁) and two double-pipe counter-flow heat exchangers (HX₂ and HX₃), and then enters the intermediate heat exchanger (HX₄) with a higher temperature after absorbing some heat in the internal loop. While in the external loop, the outer-circulating fluid absorbs the heat through the intermediate heat exchanger, and then releases it to the environment through the cooling plate, i.e., the heat radiator. In addition, a fan and four pumps use the same power system to drive the fluid flow in this system.

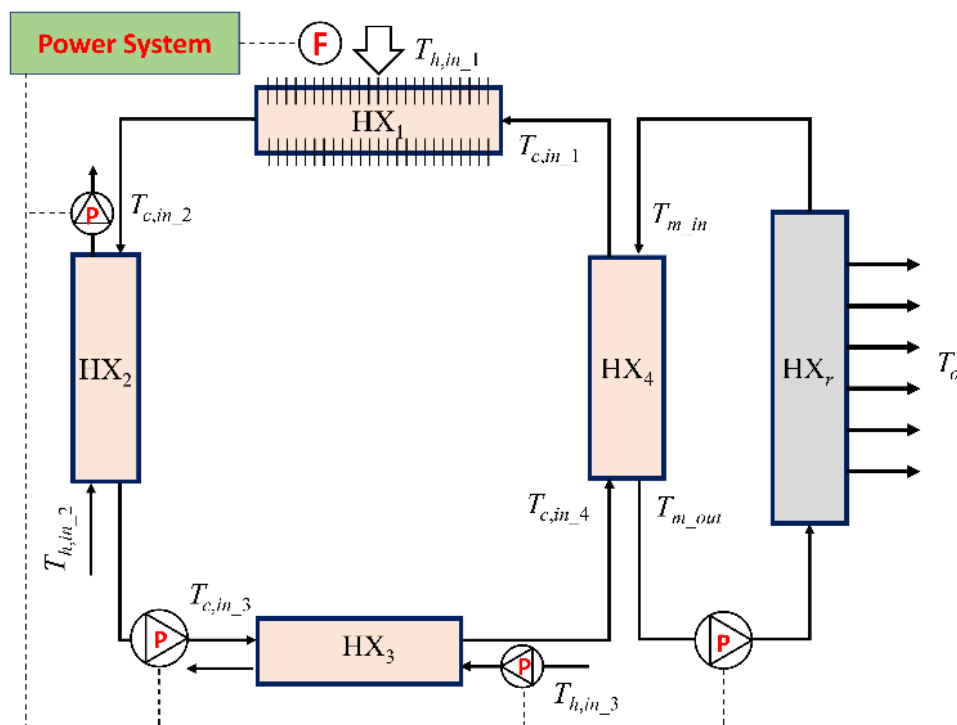


Figure 1. A typical double-loop thermal management system.

In the internal loop, the temperatures of the inner-circulating cold fluid entering HX₁, HX₂, and HX₃ are T_{c,in_1} , T_{c,in_2} , and T_{c,in_3} , respectively, and the corresponding temperatures of hot air or hot fluid are T_{h,in_1} , T_{h,in_2} , and T_{h,in_3} , respectively. In the intermediate heat exchanger, the inlet temperatures of inner-circulating and outer-circulating fluids are T_{c,in_4} , and $T_{m,in}$, respectively. The outlet temperature of the outer-circulating fluid entering HX₄ is $T_{m,out}$. Meanwhile, the outside temperature of HX_r, T_o , is kept constant in this research for simplicity.

3. The Integrated Component-System Synergy Model of Heat Transfer

3.1. The Overall Heat Current Layout of the Thermal Management System

The heat current method provides a global perspective for system modeling by considering the component performance and the system topology characteristics. According to the heat current method-based modeling solution [35,42], the overall heat current layout of the double-loop thermal

management system consists of isothermal nodes, thermal resistances, additional thermo-motive forces, and a ground connection. Figure 2 shows the heat current layout of the introduced double-loop thermal management system, including the thermal resistance element (R) and additive thermo-motive force element (ε). These two essential elements reflect the thermal energy transfer process between hot and cold fluids and the thermal energy transport process of the hot fluid or the cold fluid, respectively. Additionally, Q_1 , Q_2 , and Q_3 represent three kinds of different heat loads flowing into the system generated from the indoor environment, electric equipment, and computers with thermal resistance, R_1 , R_2 , and R_3 , respectively. The sum of three heat loads ($Q_t = Q_1 + Q_2 + Q_3$) flows through R_4 and R_r , and then is released to the isothermal node (T_o), which is similar to the ground connection in the electricity field. V_T represents the virtual thermo-motive force to keep the inlet temperatures and outside temperature constant, as shown in Figure 2.

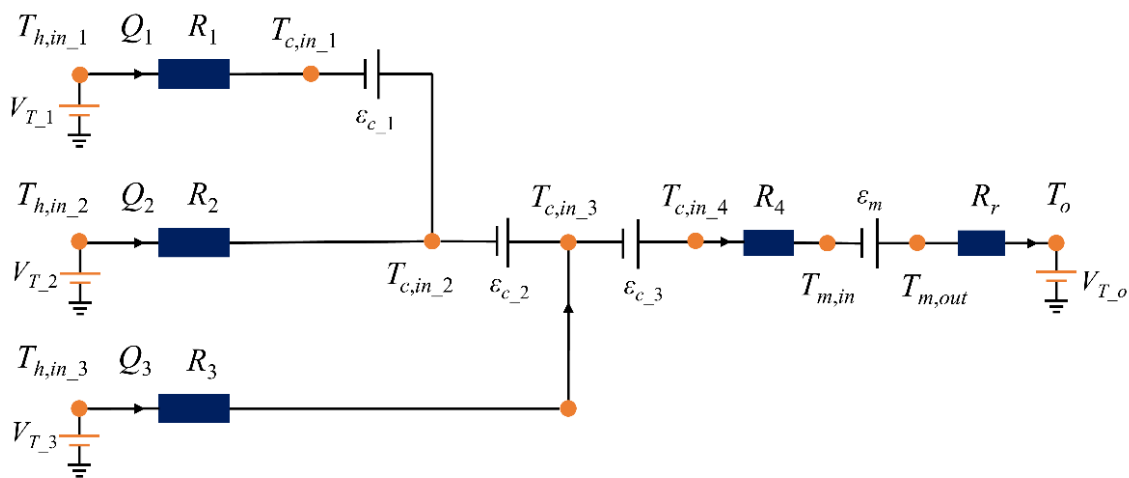


Figure 2. The heat current layout of a typical double-loop thermal management system.

On the basis of the overall heat current layout and Kirchoff' law, we can directly obtain the system-level thermal energy transfer matrix equation as follows:

$$\Delta T = RQ \tag{1}$$

where the driven potential, thermal resistance, and heat current are the following:

$$\begin{bmatrix} T_{h,in_1} - T_o \\ T_{h,in_2} - T_o \\ T_{h,in_3} - T_o \end{bmatrix} = \begin{bmatrix} R_1 + R_4 + R_r - \frac{1}{G_{in}} - \frac{1}{G_{out}} & R_4 + R_r - \frac{1}{G_{in}} - \frac{1}{G_{out}} & R_4 + R_r - \frac{1}{G_{in}} - \frac{1}{G_{out}} \\ R_4 + R_r - \frac{1}{G_{out}} & R_2 + R_4 + R_r - \frac{1}{G_{in}} - \frac{1}{G_{out}} & R_4 + R_r - \frac{1}{G_{in}} - \frac{1}{G_{out}} \\ R_4 + R_r - \frac{1}{G_{out}} & R_4 + R_r - \frac{1}{G_{out}} & R_3 + R_4 + R_r - \frac{1}{G_{in}} - \frac{1}{G_{out}} \end{bmatrix} \begin{bmatrix} Q_1 \\ Q_2 \\ Q_3 \end{bmatrix} \tag{2}$$

where G_{in} and G_{out} are the heat capacity flow rate of internal and external loop fluids, i.e., the product of the mass flow rate and specify heat capacity, respectively. R_1, R_2, R_3, R_4 , and R_r are the inlet temperature difference-based general thermal resistance, and they have the following unified expression [47]:

$$R = \frac{T_{h,in} - T_{c,in}}{Q} = \frac{G_c e^{NTU_h} - G_h e^{NTU_c}}{G_h G_c (e^{NTU_h} - e^{NTU_c})} \tag{3}$$

where NTU_h and NTU_c are the hot-end and cold-end numbers of heat transfer units in each heat exchanger, and they are the ratios of effective thermal conductance to heat capacity flow rates of hot and cold fluids:

$$\begin{aligned} NTU_h &= \frac{\varphi KA}{G_h} \\ NTU_c &= \frac{\varphi KA}{G_c} \end{aligned} \tag{4}$$

where φ is the geometric correction factor for a practical heat exchanger and represents the heat transfer degradation because of various flow arrangements as compared with a counter-flow heat exchanger, that is, the correction factor has a different calculation expression suited to a particular flow arrangement. K and A are the overall heat transfer coefficient and total heat transfer area of the heat exchanger, respectively. G_h and G_c are the heat capacity flow rates of hot and cold fluids in each heat exchanger, respectively.

When geometrical parameters of each heat exchanger are given, the mass flow rate influences the overall heat transfer coefficient of both fluids. Therefore, in this research, we introduce some empirical correlations for considering the total heat transfer coefficients and pressure drops of each heat exchanger with different flow arrangements in the thermal management system optimization. The following subsections provide the calculation expressions of heat transfer and pressure drop factors of each heat exchanger.

3.2. A Cross-Flow Plate-Fin Heat Exchanger (HX₁)

A cross-flow plate-fin heat exchanger is always available for water-air heat transfer in a double-loop heat exchanger, as shown in Figure 3. The total flow lengths of cold water and hot air are L_c and L_h , respectively. The full height of all channels of hot air and cold water is L_n . The hot-end and the cold-end fins have the same geometry as offset strip fins but different sizes. H is the fin height, W is the width between the adjacent fins, t is the fin thickness, and l is the length of each fin. These structural parameters of fins are the joint influences of the thermal-hydraulic performance of a cross-flow plate-fin heat exchanger.

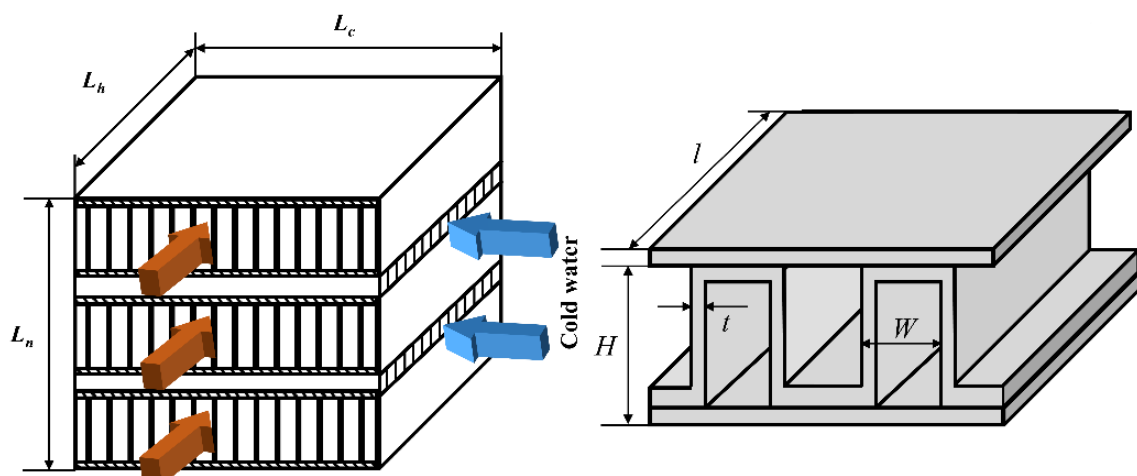


Figure 3. The sketch of the core of a plate-fin heat exchanger and the offset strip fin.

Next, in this manuscript, we apply a general thermal resistance model to describe the heat transfer process of a cross-flow plate-fin heat exchanger. In Equation (4), the correction factor φ of a cross-flow plate-fin heat exchanger can be expressed as follows [48]:

$$\varphi = \frac{\ln \left(\frac{G_{h1} \exp \left(\frac{G_{h1}}{G_{c1}} \left(e^{-\frac{(KA)_1}{G_{h1}}} - 1 \right) \right)}{G_{h1} - G_{c1} + G_{c1} \exp \left(\frac{G_{h1}}{G_{c1}} \left(e^{-\frac{(KA)_1}{G_{h1}}} - 1 \right) \right)} \right)}{\frac{(KA)_1}{G_{h1}} - \frac{(KA)_1}{G_{c1}}} \quad (5)$$

Combining with Equations (4) and (5), the general thermal resistance expression is the function of all influence factors regarding the heat transfer performance, wherein two vital parameters are the overall heat transfer coefficient (K) and the total heat transfer area (A) for the heat exchanger.

Neglecting the heat conduction resistance of the material, the thermal conductance of HX_1 is the following [49]:

$$\frac{1}{(KA)_1} = \frac{1}{\alpha_{1_h}A_{1_h}} + \frac{1}{\alpha_{1_c}A_{1_c}} \quad (6)$$

where A_{1_h} and A_{1_c} are hot-side heat transfer area and cold-side heat transfer area, respectively, and their corresponding calculations are:

$$A_{1_h} = L_h L_c N_h [1 + 2n_h(H_h - t_h)] \quad (7)$$

$$A_{1_c} = L_h L_c N_c [1 + 2n_c(H_c - t_c)] \quad (8)$$

where n_h and n_c are equal to the reciprocal of the fin width (W) of the hot side and cold side, respectively. According to [49], the expression of the total heat transfer area is as follows:

$$A_1 = A_{1_h} + A_{1_c} \quad (9)$$

Wherein, the free flow areas for the plate-fin heat exchanger of the hot and cold sides are as follows [49]:

$$A_{1_{f,h}} = L_c N_h (H_h - t_h) (1 - n_h t_h) \quad (10)$$

$$A_{1_{f,c}} = L_h N_c (H_c - t_c) (1 - n_c t_c) \quad (11)$$

Meanwhile, the convective heat transfer coefficient between the hot fluid or cold fluid and the heat exchanger plate is obtained by the following [50]:

$$\alpha_1 = j_1 M_1 c_p \text{Pr}^{-0.667} \quad (12)$$

where the mass flux velocity (M) is calculated by the ratio of mass flow rate to the free flow areas [12] as:

$$M_1 = \frac{m_1}{A_{1_{f,h}}} \quad (13)$$

In Equation (12), the parameter j_1 is the Colburn factor for both hot and cold sides with the following expression [50]:

$$j_1 = 0.6522 \text{Re}^{-0.5403} \beta^{-0.1541} \kappa^{0.1499} \gamma^{-0.0678} \left(1 + 5.269 \times 10^{-5} \text{Re}^{1.34} \beta^{0.504} \kappa^{0.456} \gamma^{-1.055}\right)^{0.1} \quad (14)$$

where β , κ , and γ are the dimensionless parameters.

$$\text{Re} = \frac{MD_1}{\mu}, \beta = \frac{W-t}{H-t}, \kappa = \frac{t}{l}, \gamma = \frac{t}{W-t} \quad (15)$$

where D_1 is the hydraulic diameter (D_{1_h} and D_{1_c}), and its expression is as follows:

$$D_1 = \frac{4(W-t)(H-t)l}{2[(W-t)l + (H-t)l + (H-t)t] + t(W-t)} \quad (16)$$

Meanwhile, the frictional pressure drop for the two fluid streams can be calculated by:

$$\Delta p_{1_h} = \frac{2f_{1_h} L_{1_h} M_{1_h}^2}{\rho_{1_h} D_{1_h}}, \Delta p_{1_c} = \frac{2f_{1_c} L_{1_c} M_{1_c}^2}{\rho_{1_c} D_{1_c}} \quad (17)$$

where the calculation expression of friction factor f_1 is [50] as follows:

$$f_1 = 9.6243 \text{Re}^{-0.7422} \beta^{-0.1856} \kappa^{0.3503} \gamma^{-0.2659} \left(1 + 7.669 \times 10^{-8} \text{Re}^{4.429} \beta^{0.920} \kappa^{3.767} \gamma^{0.236}\right)^{0.1} \quad (18)$$

Equations (14) and (18) are feasible when $120 < Re < 10^4$, $0.134 < \beta < 0.997$, $0.012 < \kappa < 0.048$, and $0.041 < \gamma < 0.121$.

3.3. Double-Pipe Counter-Flow Heat Exchangers (HX₂, HX₃, and HX₄)

In this double-loop thermal management system, HX₂, HX₃, and HX₄ are double-pipe counter-flow heat exchangers, as shown in Figure 4. For HX₂ and HX₃, the hot fluid flows through the outer tube, and the inner-circulating fluid with lower temperature flows through the inner tube. For HX₄, the circulating fluid with higher temperature flows through the inner tube, and the outer-circulating fluid flows through the outer tube. For each heat exchanger, the inside diameters of inner and outer tubes are D_{in_2} , D_{in_3} , D_{in_4} , and D_{out_2} , D_{out_3} , D_{out_4} , respectively. Meanwhile, the thickness of the tube wall of HX₂, HX₃, and HX₄ are the same, δ . The outside diameters of the inner tube are D_{m_2} ($D_{in_2} + 2\delta$), D_{m_3} ($D_{in_3} + 2\delta$), and D_{m_4} ($D_{in_4} + 2\delta$), respectively. Moreover, the total heat transfer length of HX₂, HX₃, and HX₄ are L_2 , L_3 , and L_4 , respectively.

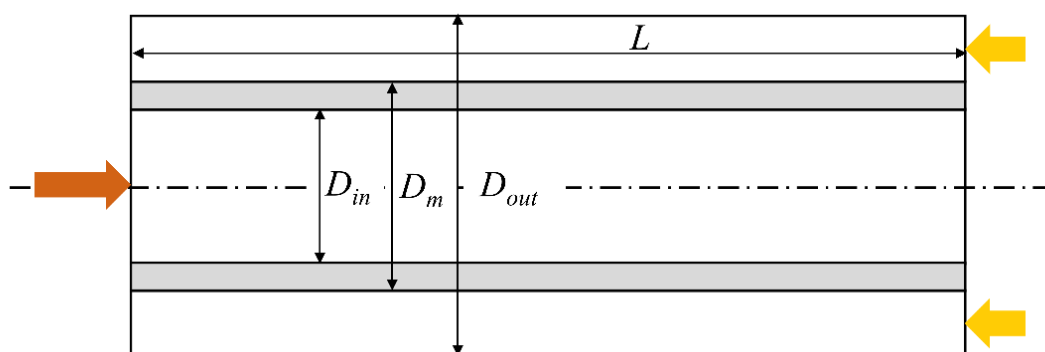


Figure 4. The sketch of the double-pipe counter-flow heat exchanger.

For each heat exchanger, the heat transfer coefficient and heat transfer area can be written as:

$$\frac{1}{K} = \frac{D_m}{D_{in}\alpha_{in}} + \frac{D_m}{2\lambda_w} \ln\left(\frac{D_m}{D_{in}}\right) + \frac{1}{\alpha_{out}} \quad (19)$$

$$A = \pi D_m L \quad (20)$$

where α_{in} and α_{out} are convective heat transfer coefficients of the inner tube and outer tube, and their expressions are the following:

$$\alpha_{in} = \frac{\lambda_{in} Nu_{w_in}}{D_{in}} \quad (21)$$

$$\alpha_{out} = \frac{\lambda_{out} Nu_{w_out}}{(D_{out} - D_m)} \quad (22)$$

For the fluids of inner and outer tubes, the Nu can be calculated by the empirical correlation given by Gnielinsk's equation [50] as:

$$Nu_w = \frac{\frac{f_w}{8} (Re_w - 1000) Pr_w}{1 + 12.7 \left(\frac{f_w}{8}\right)^{0.5} (Pr_w^{2/3} - 1)} \quad (23)$$

where Re_w and Pr_w are the Reynolds number and Prandtl number. f_w is a friction factor and is calculated by:

$$f_w = (1.82 \log Re_w - 1.64)^{-2} \quad (24)$$

The pressure drop expression, of the fluid flowing in each tube, is as follows:

$$\Delta p = \frac{f_w L M^2}{2\rho D} \quad (25)$$

3.4. A Cooling-Plate Heat Exchanger (HX_r)

In the external loop, HX_r is a cooling-plate heat exchanger, as shown in Figure 5, i.e., a radiator for releasing the heat to the environment with assumed constant temperature. In the analysis, the total heat transfer area is A_r , the circulating fluid in the external loop with high temperature is divided into n parallel parts, and then enters the radiator to transfer the heat, and the hot fluid flows through the cooling plate and cooled by the lower outside temperature. Equations (21) and (25) can calculate the heat transfer coefficient and pressure drop, respectively. When the temperature of the cold side is constant, the thermal resistance of the cooling plate can be written as:

$$R_r = \frac{e^{NTU_h}}{G_h(e^{NTU_h} - 1)} \quad (26)$$

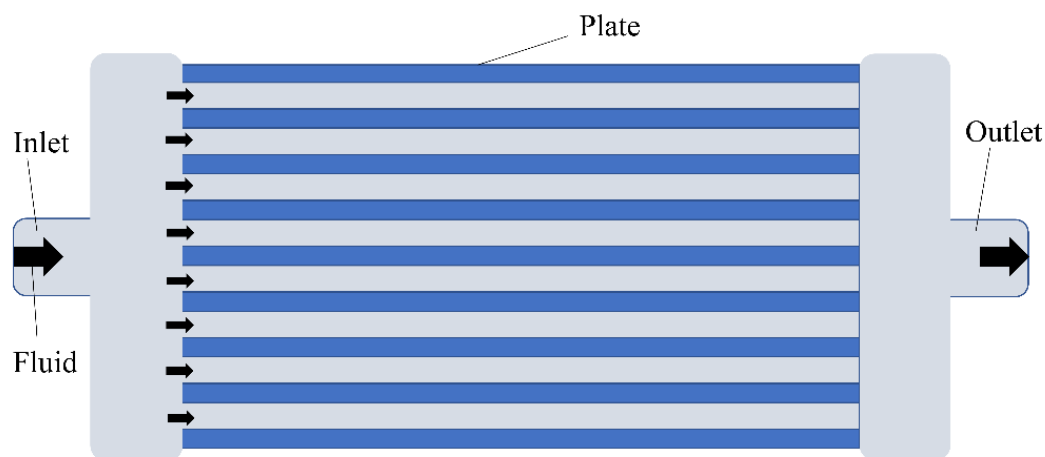


Figure 5. The sketch of the cooling-plate heat exchanger.

4. Optimization Model and Process

4.1. Optimization Objective

For a typical double-loop thermal management system used for battery cooling, spacecraft thermal control, or data center/building cooling, the minimum operational cost is always beneficial in the thermal management system applications, and thus has received more attention. In general, the operating cost is related to the pump power or the fan power to overcome the flow resistance of each fluid. Therefore, the optimization objective is the minimum total pressure drop caused by the flow resistance:

$$\min(\Delta p_t) = \min \sum \Delta p_1 + \Delta p_2 + \Delta p_3 + \Delta p_4 + \Delta p_r \quad (27)$$

where Δp_1 , Δp_2 , Δp_3 , Δp_4 , and Δp_r are total pressure drops of both hot and cold fluids of HX_1 , HX_2 , HX_3 , HX_4 , and HX_r , respectively. The total mass flow rate is rated as:

$$m_t = m_{h1} + m_{h2} + m_{h3} + m_{in} + m_{out} \quad (28)$$

where m_{h1} , m_{h2} , and m_{h3} are mass flow rates of each hot fluid in HX_1 , HX_2 , and HX_3 , respectively. m_{in} and m_{out} are mass flow rates of internal and external loop fluids, respectively.

4.2. Optimization Process

Combining with the system heat transfer constraint expressed in Equation (2), the optimization problem of the minimum total pressure drop is a typical conditional extremum problem. With the constraint of the rated total mass flow rate, a Lagrange function J is constructed as:

$$\begin{aligned}
 J = & (\Delta p_1 + \Delta p_2 + \Delta p_3 + \Delta p_4 + \Delta p_r) \\
 & + \theta_1 \left[T_{h,in_1} - T_o - \left(Q_1 R_1 + Q_t R_4 + Q_t R_r - \frac{Q_t}{m_{in} c_p} - \frac{Q_t}{m_{out} c_p} \right) \right] \\
 & + \theta_2 \left[T_{h,in_2} - T_o - \left(Q_2 R_2 + Q_t R_4 + Q_t R_r - \frac{Q_2 + Q_3}{m_{in} c_p} - \frac{Q_t}{m_{out} c_p} \right) \right] \\
 & + \theta_3 \left[T_{h,in_3} - T_o - \left(Q_3 R_3 + Q_t R_4 + Q_t R_r - \frac{Q_3}{m_{in} c_p} - \frac{Q_t}{m_{out} c_p} \right) \right] \\
 & + \theta_4 (m_t - m_{h1} - m_{h2} - m_{h3} - m_{in} - m_{out})
 \end{aligned} \tag{29}$$

where θ_1 , θ_2 , θ_3 , and θ_4 are Lagrange multipliers, respectively. Making the differential of J with respect to each variable equal to zero gives the following:

$$\frac{\partial J}{\partial X_l} = 0, X_l \in [m_{h1}, m_{h2}, m_{h3}, m_{in}, m_{out}, \theta_1, \theta_2, \theta_3, \theta_4] \tag{30}$$

These equations contain nine variables, i.e., the mass flow rate of each working fluid and four Lagrange multipliers. Solving these equations expressed in Equation (30) will obtain the optimal results.

5. Synergy Optimization Results and Discussions

5.1. The Simulation Calculation Cases

Here, we present the analysis and optimization of the thermal management system under some necessary given conditions. The heat loads of HX₁, HX₂, and HX₃ are 4000, 6000, and 2000 W, respectively. Meanwhile, the inlet temperatures of hot fluids flowing into HX₁, HX₂, and HX₃ are 340, 330, and 320 K, respectively. The cooling-plate temperature remains constant, at 275 K. For the cross-flow plate-fin heat exchanger HX₁, the total flow length of the cold-end and hot-end are 0.12 and 0.11 m, respectively. Table 1 gives the fin width, height, length, and thickness of the hot-air side and cold-water side. The fin number of the hot-side and cold-side are 7 and 8, respectively. Moreover, the inner diameter of the internal pipe of HX₂, HX₃, and HX₄ is the same, i.e., 20 mm. The tube wall thickness is 2 mm of each counter-flow heat exchanger. The inner diameters of the external pipe of HX₂, HX₃, and HX₄ are 50, 50, and 60 mm, respectively.

Table 1. Some given geometrical parameters of HX₁.

| Cold-Water Side | Value (mm) | Hot-Air Side | Value (mm) |
|---------------------|------------|---------------------|------------|
| Width (W_c) | 3 | Width (W_h) | 2 |
| Height (H_c) | 3 | Height (H_h) | 9 |
| Length (l_c) | 3 | Length (l_h) | 4 |
| Thickness (t_c) | 0.1 | Thickness (t_h) | 0.15 |

Under the given conditions, when the mass flow rate of the fluid in the external loop is 0.5 kg/s, we simulate the thermal management system and obtain the working temperatures of the internal and external fluids, as shown in Table 2. The minimum and maximum temperatures of the internal fluid are 277.05 and 317.77 K. The temperature of the external fluid decreases from 282.76 to 277.02 K by releasing the heat through the cooling-plate heat exchanger. Meanwhile, the mass flow rates of hot fluid in HX₁, HX₂, HX₃, and HX₄ are 0.097, 0.08, 0.253, and 0.07 kg/s, respectively. The total pressure drop of this system is 68.71 KPa. The simulation results show that the combination of heat current

method and empirical correlations is feasible and convenient for the combined component-system synergy analysis.

Table 2. Simulation temperatures of the internal loop and external loop fluids.

| T_{c,in_1} (K) | T_{c,in_2} (K) | T_{c,in_3} (K) | T_{c,in_4} (K) | $T_{m,in}$ (K) | $T_{m,out}$ (K) |
|------------------|------------------|------------------|------------------|----------------|-----------------|
| 277.05 | 290.62 | 310.98 | 317.77 | 277.02 | 282.76 |

5.2. Synergy Optimization Results

When the structural parameters of each heat exchanger are given and shown in the above entries, we obtain the optimal mass flow distribution when the total mass flow rate is 1 kg/s, by solving these equations showed in Equation (29). Meanwhile, numerical simulation cases and results under different mass flow rates of the external fluid are obtained and pictured in Figure 6. Compared with simulation cases, the total pressure drop, using the proposed optimization method, is the minimum. After the optimization, the mass flow rates of hot fluids in HX_1 , HX_2 , and HX_3 are 0.099, 0.083, and 0.426 kg/s, respectively. The mass flow rates of fluids flowing through internal and external loops are 0.071 and 0.321 kg/s. The minimum pressure drop is 63.14 kPa, reducing 8.1% as compared with the above simulation result when the mass flow rate of the fluid in the external loop is 0.5 kg/s. Meanwhile, the thermal resistances of each heat exchanger are 0.0083, 0.0032, 0.0020, 0.0029, and 0.003 K/W, respectively, that is, the optimal allocation of the mass flow rate of fluids in the thermal management system is necessary for reducing the total pressure drop and the operational cost.

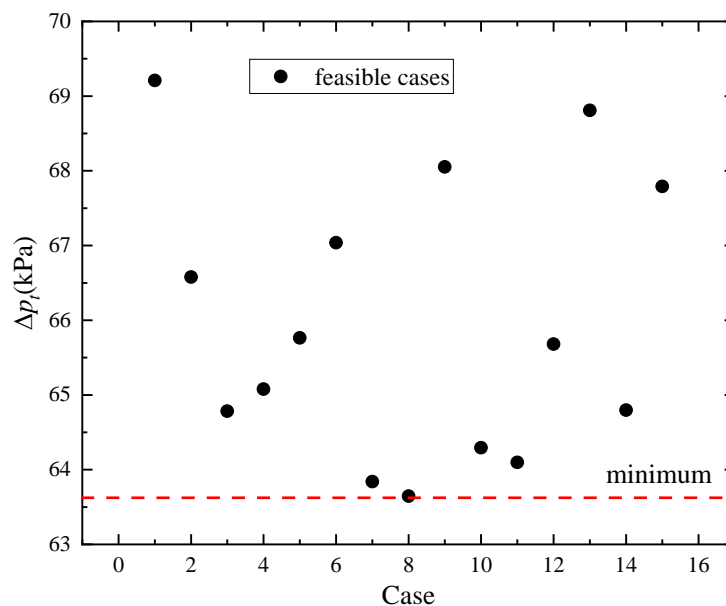


Figure 6. The feasible cases and the minimum pressure drop.

5.3. Parameters Analysis and Discussions

For the introduced typical double-loop thermal management system, any one structural parameter, operational parameter, and boundary condition can generate influence on optimization results. Therefore, the following parts show the impact analysis of such factors as the fin width of the cross-flow plate-fin heat exchanger, the inlet temperatures, the heat load, and the total mass flow rate.

Figure 7 presents these variations of the total pressure drop and mass flow rates of each fluid in a thermal management system with an increase in fin width of the cold-water side in HX_1 . Wherein, the total pressure drop decreases from 63.21 to 63.08 kPa when the fin width increases from 2.5 mm to 3.5 mm. Meanwhile, the mass flow rates of the internal loop fluid and hot fluids in HX_2 and HX_3 keep

constant. The mass flow rates of hot fluid in HX_1 and the external loop fluid will increase and decrease, respectively. Consequently, an increase in the fin width of the cold-water side is a benefit to reduce the total pressure drop of the thermal management system and generate some minor impacts on the optimal allocation of mass flow rate.

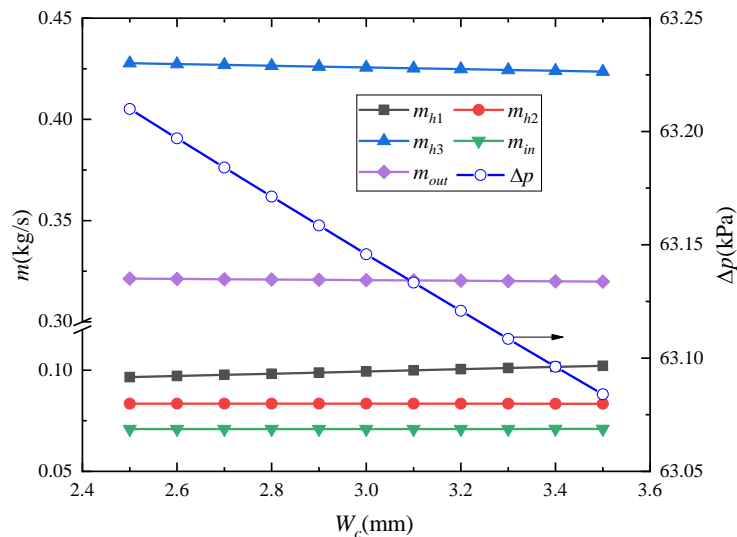


Figure 7. The total pressure drop and mass flow rate vary with the fin width (W_c) of the cold-water side in HX_1 .

Moreover, Figure 8 shows these influences of the fin width of the hot-air side in HX_1 on the optimization results. When the fin width of the hot-air side increases from 1.5 mm to 2.5 mm, the total pressure drop reduces from 63.63 kPa to 62.63 kPa, about 1 kPa. Since an increase in the fin width of the hot-air side reduces the convective heat transfer coefficient, the mass flow rate of hot air increases by 38.7% for keeping the same heat transfer ability. Meanwhile, the mass flow rates of fluid in the external loop and that of the hot fluid in HX_3 both decrease, while the mass flow rate of other fluids has a minor variation. Therefore, an increase in the fin width of the hot-air side is more effective for reducing total pressure drop and the total operational cost. Meanwhile, according to Figures 7 and 8, these optimization results show that variations of local geometrical parameters of the heat exchanger influence the optimal operation of other heat transfer components.

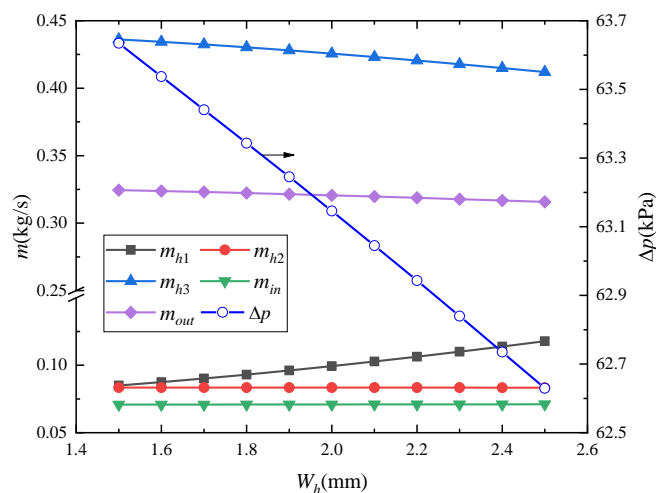


Figure 8. The total pressure drop and mass flow rate vary with the fin width (W_h) of the hot-air side in HX_1 .

When the inlet temperature of hot fluid in each heat exchanger varies with the heat load, the optimal allocation of mass flow rates changes. As shown in Figure 9, the total pressure drop increases about 0.55 kPa and the mass flow rate of the hot air in HX_1 decreases 22.68%, when the inlet temperature of the hot air in HX_1 increases from 335 K to 345 K. According to the definition of inlet temperature difference-based thermal resistance, due to a rise in the inlet temperature of hot fluid, the driven potential for heat transfer will increase. Under the same heat load, the thermal resistance increases with a decrease in the mass flow rate of hot fluid. Meanwhile, the optimal mass flow rates of the hot fluid in HX_3 and the external loop fluid increase due to an increase in the inlet temperature of hot air in the HX_1 .

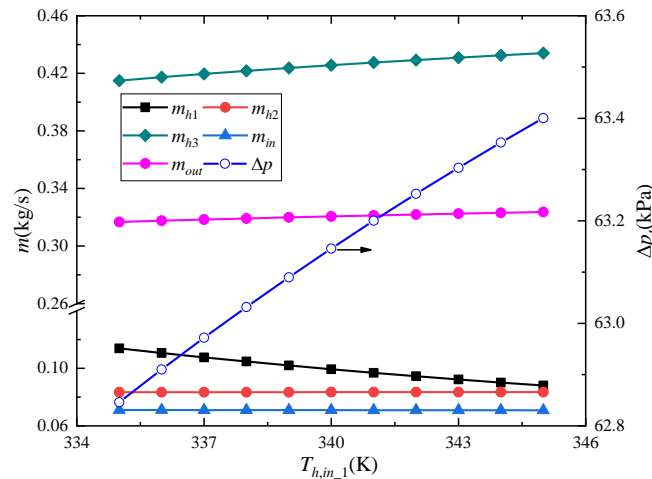


Figure 9. The total pressure drop and mass flow rate vary with the inlet temperature of hot air in HX_1 .

Moreover, Figure 10 presents variations of the total pressure drop and mass flow rates of each fluid in the thermal management system with an increase in the inlet temperature of the hot fluid in HX_3 . Because the location of HX_3 is different from the HX_1 in the thermal management system, the variation of the inlet temperature of the hot fluid in HX_3 will bring different trends. The total pressure drop will reduce about 2.41 kPa when the inlet temperature of the hot fluid (T_{h,in_3}) increases 10 K under the same load. Compared with the inlet temperature of the hot fluid (T_{h,in_1}) in HX_1 , T_{h,in_3} will have a more distinct influence on the total operational cost. Meanwhile, the optimal allocation of mass flow rates is different. The mass flow rates of the internal loop and external loop fluids all reduce, and the mass flow rates of hot fluids in HX_2 and HX_3 increase, respectively.

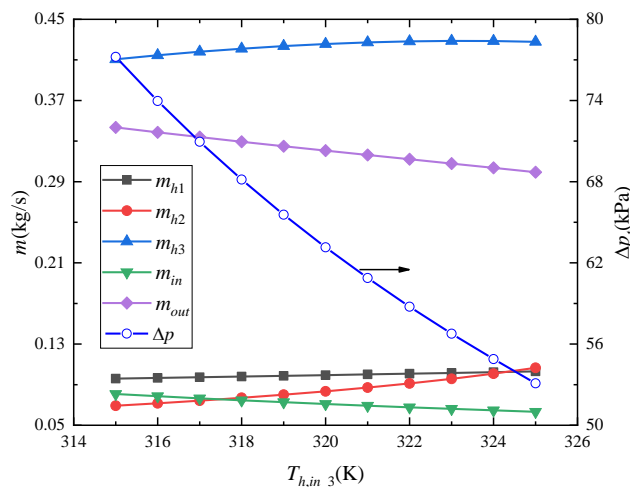


Figure 10. The total pressure drop and mass flow rate vary with the inlet temperature of the hot fluid in HX_3 .

In addition, Figure 11 shows that the total pressure drop and the optimal allocation of the mass flow rate vary with an increase in the heat load of HX₂. When the heat load of HX₂ increases, the total pressure drop increases, that is, the total operational costs increase with a rise in the heat load of HX₂. Meanwhile, the mass flow rates of the hot fluids in HX₂ and HX₃ increase and decrease, respectively. Therefore, the variation of local heat load generates an influence on the optimal allocation of the mass flow rate. Finally, when the total mass flow rate increases, due to the increase in the mass flow rates of the fluids in HX₃ and the external loop, Figure 12 shows that the optimal total pressure drop increases from 60.6 to 66.54 kPa.

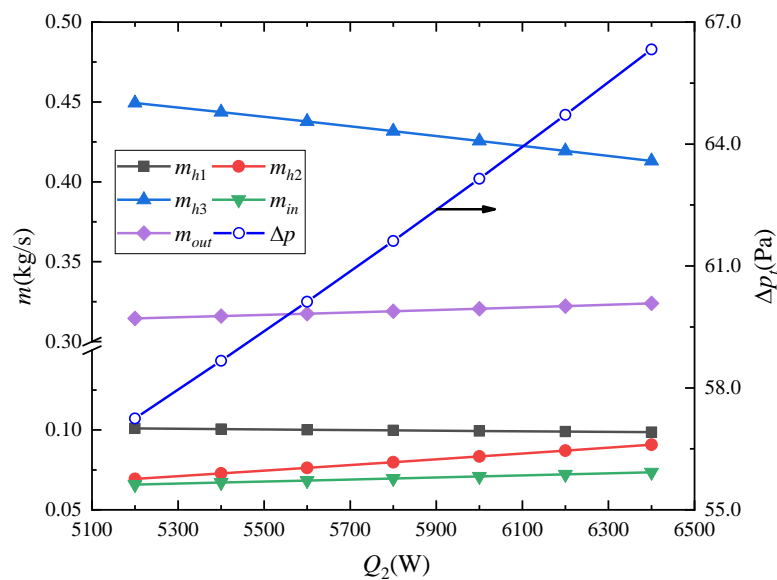


Figure 11. The total pressure drop and mass flow rate vary with the heat load in HX₂.

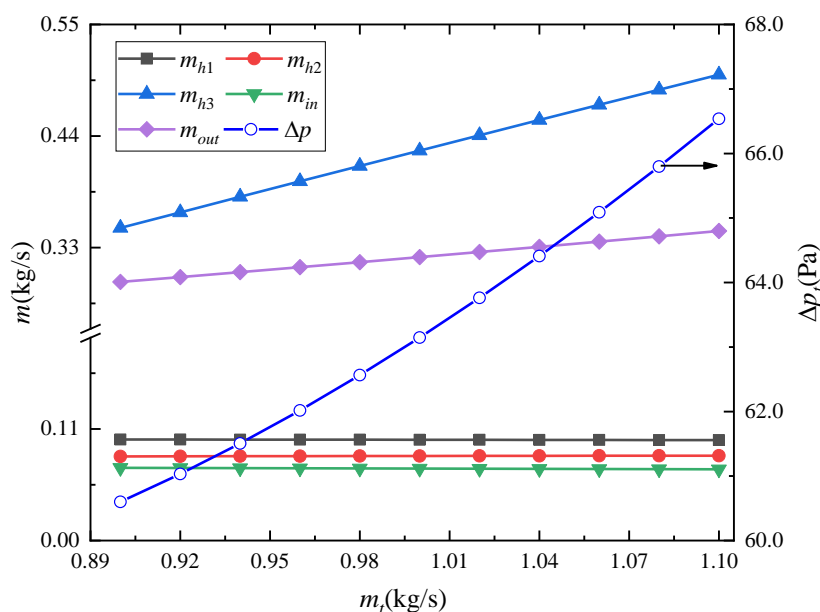


Figure 12. The total pressure drop and mass flow rate of each fluid vary with the total mass flow rate.

The above-combined simulation and optimization of components and systems are achieved by combining the heat current method for system-level analysis with the empirical correlations for component-level analysis. For each heat transfer component, the heat transfer performance and fluid flow characteristic are described by the empirical correlations obtained by the experiment results. Besides, the system typology characteristic is described using the heat current layout combining with

Kirchhoff's law. In this framework, the intermediate temperatures of the circulating fluid in internal and external loops are omitted, and thus benefit the holistic analysis and synergy optimization.

6. Conclusions

Integration modeling and optimization of component and system provide a holistic perspective for thermal management system design and optimization. This contribution introduced a typical double-loop thermal management system and applied the heat current method for constructing its overall heat current layout, and then deduced the heat transfer matrix by Kirchhoff's law. In the deduced heat transfer matrix, the network thermal resistance reflects the component performance and system typology characteristic. Moreover, we introduced some empirical correlations of heat transfer and pressure drop to consider the influences of structural and operational parameters of each heat transfer component on the system overall performance. The combination of the general thermal resistance and the empirical correlation provides a new solution for optimizing the component structure at the system level.

Furthermore, the research provided a simulation case and optimization case for validating the proposed component-system modeling and optimization method. Solving these optimal governing equations derived by the Lagrange multiplier method with consideration of the physical constraints and operational conditions shows that the minimum pressure drop reduces about 8.1% with the optimal allocation of mass flow rates of each fluid. In addition, a variation of the local geometrical parameters of the heat exchanger influences the optimal operation of other heat transfer components. Consequently, the consideration of the heat exchanger structural parameters in system-level optimization can be achieved by combining the heat current method and the empirical correlation. This combination provided a feasible and significant solution for the integrated component-system optimization for the thermal management system.

Author Contributions: Conceptualization, methodology, investigation, writing—original draft preparation, J.H.; software and validation, Y.Z. and N.X. All authors have read and agreed to the published version of the manuscript.

Funding: This research received no external funding.

Acknowledgments: The authors would like to thank the Fundamental Research Funds for the Central Universities (2020MS010), the National Natural Science Foundation of China (grant no. 51806119).

Conflicts of Interest: The authors declare no conflict of interest.

Correction Statement: This article has been republished with a minor change. The change does not affect the scientific content of the article and further details are available within the backmatter of the website version of this article.

Nomenclatures

| | |
|-------|--|
| A | area, m^2 |
| c_p | specific heat capacity, $J\ kg^{-1}\ K^{-1}$ |
| D | hydraulic diameter, m |
| f | friction factor |
| G | heat capacity rate flow, $G = mc_p$, $W\ K^{-1}$ |
| H | height, m |
| j | Colburn factor |
| J | Lagrange function |
| K | overall heat transfer coefficient, $W\ m^{-2}\ K^{-1}$ |
| l | length of a single fin, m |
| L | total length, m |
| m | mass flow rate, $kg\ s^{-1}$ |
| M | mass flux velocity, $kg\ m^{-2}\ s^{-1}$ |
| n | fin frequency, m^{-1} |

| | |
|---------------|---|
| N | channel number |
| Nu | Nusselt number |
| p | pressure, Pa |
| Pr | Pr number |
| Q | heat flux, W |
| R | thermal resistance, $K W^{-1}$ |
| Re | Re number |
| t | thickness, m |
| T | temperature, K |
| V | virtual thermo-motive force |
| W | width, m |
| α | convective heat transfer coefficient, $W m^{-2} K^{-1}$ |
| β | dimensionless parameter |
| δ | thickness, mm |
| γ | dimensionless parameter |
| κ | dimensionless parameter |
| λ | thermal conductivity, $W K^{-1} m^{-1}$ |
| ρ | density, $kg m^{-3}$ |
| φ | correction factor |
| θ | Lagrange multiplier |
| ε | additive thermo-motive force, K subscripts |
| a | air |
| c | cold fluid |
| h | hot fluid |
| in | inner, inlet |
| m | intermediate heat exchanger |
| out | outer, outlet |
| r | radiator |
| t | total |
| w | water |

References

1. Chainer, T.J.; Schultz, M.D.; Parida, P.R.; Gaynes, M.A. Improving data center energy efficiency with advanced thermal management. *IEEE Trans. Compon. Packag. Manuf. Technol.* **2017**, *7*, 1228–1239. [[CrossRef](#)]
2. Tyagi, V.; Pandey, A.; Buddhi, D.; Kothari, R. Thermal performance assessment of encapsulated PCM based thermal management system to reduce peak energy demand in buildings. *Energy Build.* **2016**, *117*, 44–52. [[CrossRef](#)]
3. Ye, Y.; Saw, L.H.; Shi, Y.; Tay, A.A. Numerical analyses on optimizing a heat pipe thermal management system for lithium-ion batteries during fast charging. *Appl. Therm. Eng.* **2015**, *86*, 281–291. [[CrossRef](#)]
4. Ye, Y.; Shi, Y.; Saw, L.H.; Tay, A.A. Performance assessment and optimization of a heat pipe thermal management system for fast charging lithium ion battery packs. *Int. J. Heat Mass Transf.* **2016**, *92*, 893–903. [[CrossRef](#)]
5. Chen, K.; Wu, W.; Yuan, F.; Chen, L.; Wang, S. Cooling efficiency improvement of air-cooled battery thermal management system through designing the flow pattern. *Energy* **2019**, *167*, 781–790. [[CrossRef](#)]
6. Mason, J.A.; Oktawiec, J.; Taylor, M.K.; Hudson, M.R.; Rodriguez, J.; Bachman, J.E.; Gonzalez, M.I.; Cervellino, A.; Guagliardi, A.; Brown, C.M. Methane storage in flexible metal—Organic frameworks with intrinsic thermal management. *Nature* **2015**, *527*, 357. [[CrossRef](#)]
7. Lee, S.; Mudawar, I.; Hasan, M.M. Thermal analysis of hybrid single-phase, two-phase and heat pump thermal control system (TCS) for future spacecraft. *Appl. Therm. Eng.* **2016**, *100*, 190–214. [[CrossRef](#)]
8. Wang, J.-X.; Li, Y.-Z.; Zhang, H.-S.; Wang, S.-N.; Liang, Y.-H.; Guo, W.; Liu, Y.; Tian, S.-P. A highly self-adaptive cold plate for the single-phase mechanically pumped fluid loop for spacecraft thermal management. *Energy Convers. Manag.* **2016**, *111*, 57–66. [[CrossRef](#)]

9. Smith, K.; Wang, C.-Y. Power and thermal characterization of a lithium-ion battery pack for hybrid-electric vehicles. *J. Power Sour.* **2006**, *160*, 662–673. [[CrossRef](#)]
10. Chen, H.; Pei, P.; Song, M. Lifetime prediction and the economic lifetime of proton exchange membrane fuel cells. *Appl. Energy* **2015**, *142*, 154–163. [[CrossRef](#)]
11. O'hayre, R.; Cha, S.-W.; Prinz, F.B.; Colella, W. *Fuel Cell Fundamentals*; John Wiley & Sons: Hoboken, NJ, USA, 2016.
12. Shah, R.K.; Sekulic, D.P. *Fundamentals of Heat Exchanger Design*; John Wiley & Sons: Hoboken, NJ, USA, 2003.
13. Jaluria, Y. *Design and Optimization of Thermal Systems*; CRC Press: Boca Raton, FL, USA, 2007.
14. Bhutta, M.M.A.; Hayat, N.; Bashir, M.H.; Khan, A.R.; Ahmad, K.N.; Khan, S. CFD applications in various heat exchangers design: A review. *Appl. Therm. Eng.* **2012**, *32*, 1–12. [[CrossRef](#)]
15. Kakac, S.; Liu, H.; Pramuanjaroenkij, A. *Heat Exchangers: Selection, Rating, and Thermal Design*; CRC Press: Boca Raton, FL, USA, 2012.
16. Eldeeb, R.; Aute, V.; Radermacher, R. A survey of correlations for heat transfer and pressure drop for evaporation and condensation in plate heat exchangers. *Int. J. Refrig.* **2016**, *65*, 12–26. [[CrossRef](#)]
17. Braz Filho, F.A.; Fortes, M.A.; Ribeiro, G.B. Comparison of interfacial heat transfer correlations for high-pressure subcooled boiling flows via CFD two-fluid model. *J. Braz. Soc. Mech. Sci. Eng.* **2019**, *41*, 307. [[CrossRef](#)]
18. Huang, S.; Ma, Z.; Cooper, P. Optimal design of vertical ground heat exchangers by using entropy generation minimization method and genetic algorithms. *Energy Convers. Manag.* **2014**, *87*, 128–137. [[CrossRef](#)]
19. Ayala, H.V.H.; Keller, P.; de Fátima Morais, M.; Mariani, V.C.; dos Santos Coelho, L.; Rao, R.V. Design of heat exchangers using a novel multiobjective free search differential evolution paradigm. *Appl. Therm. Eng.* **2016**, *94*, 170–177. [[CrossRef](#)]
20. Wen, J.; Yang, H.; Tong, X.; Li, K.; Wang, S.; Li, Y. Configuration parameters design and optimization for plate-fin heat exchangers with serrated fin by multi-objective genetic algorithm. *Energy Convers. Manag.* **2016**, *117*, 482–489. [[CrossRef](#)]
21. Hamut, H.; Dincer, I.; Naterer, G. Performance assessment of thermal management systems for electric and hybrid electric vehicles. *Int. J. Energy Res.* **2013**, *37*, 1–12. [[CrossRef](#)]
22. Cheng, X.; Liang, X. Discussion on the applicability of entropy generation minimization to the analyses and optimizations of thermodynamic processes. *Energy Convers. Manag.* **2013**, *73*, 121–127. [[CrossRef](#)]
23. Hamut, H.; Dincer, I.; Naterer, G. Exergy analysis of a TMS (thermal management system) for range-extended EVs (electric vehicles). *Energy* **2012**, *46*, 117–125. [[CrossRef](#)]
24. Javani, N.; Dincer, I.; Naterer, G.; Yilbas, B. Exergy analysis and optimization of a thermal management system with phase change material for hybrid electric vehicles. *Appl. Therm. Eng.* **2014**, *64*, 471–482. [[CrossRef](#)]
25. Li, T.; Yuan, Z.; Xu, P.; Zhu, J. Entropy dissipation/loss-based optimization of two-stage organic Rankine cycle (TSORC) with R245fa for geothermal power generation. *Sci. China Technol. Sci.* **2016**, *59*, 1524–1536. [[CrossRef](#)]
26. Han, Y.; Wang, D.; Zhang, C.; Zhu, Y. The entropy degeneration and entropy loss equations for the generalized irreversible Carnot engine system. *Int. J. Heat Mass Transf.* **2017**, *106*, 895–907. [[CrossRef](#)]
27. Braimakis, K.; Karellas, S. Integrated thermoeconomic optimization of standard and regenerative ORC for different heat source types and capacities. *Energy* **2017**, *121*, 570–598. [[CrossRef](#)]
28. Dixit, M.; Arora, A.; Kaushik, S. Thermodynamic and thermoeconomic analyses of two stage hybrid absorption compression refrigeration system. *Appl. Therm. Eng.* **2017**, *113*, 120–131. [[CrossRef](#)]
29. Wang, J.-J.; Jing, Y.-Y.; Zhang, C.-F. Optimization of capacity and operation for CCHP system by genetic algorithm. *Appl. Energy* **2010**, *87*, 1325–1335. [[CrossRef](#)]
30. Peng, F.; Cui, G. Efficient simultaneous synthesis for heat exchanger network with simulated annealing algorithm. *Appl. Therm. Eng.* **2015**, *78*, 136–149. [[CrossRef](#)]
31. Arat, H.; Arslan, O. Optimization of district heating system aided by geothermal heat pump: A novel multistage with multilevel ANN modelling. *Appl. Therm. Eng.* **2017**, *111*, 608–623. [[CrossRef](#)]
32. Patel, V.K.; Savsani, V.J.; Tawhid, M.A. *Thermal System Optimization: A Population-Based Metaheuristic Approach*; Springer: Berlin/Heidelberg, Germany, 2019.

33. Fiaschi, D.; Manfrida, G.; Russo, L.; Talluri, L. Improvement of waste heat recuperation on an industrial textile dryer: Redesign of heat exchangers network and components. *Energy Convers. Manag.* **2017**, *150*, 924–940. [[CrossRef](#)]
34. Liu, D.; Chen, Q.; He, K.-L.; Chen, X. An integrated system-level and component-level optimization of heat transfer systems based on the heat current method. *Int. J. Heat Mass Transf.* **2019**, *131*, 623–632. [[CrossRef](#)]
35. Hao, J.; Ge, W.; Chen, Q.; He, K.; Luo, H.; Zhou, G. Power Flow Method-Based Integrated Modeling and Optimization for Building Heat Transport and Gas Refrigeration System. *J. Energy Eng.* **2018**, *144*, 04018060. [[CrossRef](#)]
36. Do, K.H.; Choi, B.-I.; Han, Y.-S.; Kim, T. Experimental investigation on the pressure drop and heat transfer characteristics of a recuperator with offset strip fins for a micro gas turbine. *Int. J. Heat Mass Transf.* **2016**, *103*, 457–467. [[CrossRef](#)]
37. Zarea, H.; Kashkooli, F.M.; Mehryan, A.M.; Saffarian, M.R.; Beherghani, E.N. Optimal design of plate-fin heat exchangers by a Bees Algorithm. *Appl. Therm. Eng.* **2014**, *69*, 267–277. [[CrossRef](#)]
38. Yousefi, M.; Enayatifar, R.; Darus, A. Optimal design of plate-fin heat exchangers by a hybrid evolutionary algorithm. *Int. Commun. Heat Mass Transf.* **2012**, *39*, 258–263. [[CrossRef](#)]
39. Guo, Z.; Zhu, H.; Liang, X. Entransy—A physical quantity describing heat transfer ability. *Int. J. Heat Mass Transf.* **2007**, *50*, 2545–2556. [[CrossRef](#)]
40. Chen, Q. Entransy dissipation-based thermal resistance method for heat exchanger performance design and optimization. *Int. J. Heat Mass Transf.* **2013**, *60*, 156–162. [[CrossRef](#)]
41. Chen, Q.; Hao, J.; Fu, R.; Wang, Y.; Zhao, S.; Zhao, T. Entransy-based power flow method for analysis and optimization of thermal systems. *J. Eng. Thermophys.* **2017**, *38*, 1–8.
42. Chen, Q.; Hao, J.; Zhao, T. An alternative energy flow model for analysis and optimization of heat transfer systems. *Int. J. Heat Mass Transf.* **2017**, *108*, 712–720. [[CrossRef](#)]
43. Hao, J.; Chen, Q.; Ren, J.; Zhang, M.; Ai, J. An experimental study on the fin geometry optimization of a plate-fin heat exchanger based on the heat current model. *Appl. Therm. Eng.* **2019**, *154*, 111–119. [[CrossRef](#)]
44. Zhang, M.-Q.; Chen, Q.; Shao, W.; Chen, X.; Hao, J.-H. An integral identification method of characteristic parameters and optimization of parallel connection heat transfer systems based on the power flow method. *Appl. Therm. Eng.* **2018**, *143*, 1057–1067. [[CrossRef](#)]
45. Hao, J.-H.; Chen, Q.; Li, X.; Zhang, M.-Q.; Yuan, F. A new modeling and analysis method of the indirect evaporative heat exchanger based on the heat current perspective. *Appl. Therm. Eng.* **2019**, *163*, 114331. [[CrossRef](#)]
46. Hao, J.-H.; Ge, Z.-H.; Chen, Q.; Li, X.; Du, X.-Z. The coupled process-component modeling and optimization for heat exchanger of supercritical CO₂ with property variation based on heat current method. *Appl. Therm. Eng.* **2019**, *168*, 114833. [[CrossRef](#)]
47. Hao, J.-H.; Li, X.; Chen, Q. *A General Thermal Resistance with Correction Factor for Heat Exchanger Design and Analysis Based on Power Flow Method*; International Heat Transfer Conference Digital Library; Begel House Inc.: Los Angeles, CA, USA, 2018.
48. Patel, V.; Savsani, V. Optimization of a plate-fin heat exchanger design through an improved multi-objective teaching-learning based optimization (MO-ITLBO) algorithm. *Chem. Eng. Res. Des.* **2014**, *92*, 2371–2382. [[CrossRef](#)]
49. Manglik, R.M.; Bergles, A.E. Heat transfer and pressure drop correlations for the rectangular offset strip fin compact heat exchanger. *Exp. Therm. Fluid Sci.* **1995**, *10*, 171–180. [[CrossRef](#)]
50. Bergman, T.L.; Incropera, F.P.; DeWitt, D.P.; Lavine, A.S. *Fundamentals of Heat and Mass Transfer*; John Wiley & Sons: Hoboken, NJ, USA, 2011.

Publisher’s Note: MDPI stays neutral with regard to jurisdictional claims in published maps and institutional affiliations.



© 2020 by the authors. Licensee MDPI, Basel, Switzerland. This article is an open access article distributed under the terms and conditions of the Creative Commons Attribution (CC BY) license (<http://creativecommons.org/licenses/by/4.0/>).